Analysis of gamma-ray and neutron-induced chromosome aberrations in CHO-K1 cells using the atomic force microscope

M. Meincken[a*], B.S. Smit[b], R.D. Sanderson[a] and J.P. Slabbert[b]

THE ENUMERATION OF CHROMOSOME aberrations remains a popular method to relate DNA damage to radiation dose delivered, and is the basis of efforts to improve aberration assays. In the work reported here, atomic force microscopy was used to study the induction of chromosome aberrations in CHO-K1 cells, after irradiation with 1–3 Gy p(66)/Be neutrons and 2–7 Gy ^{60}Co γ-rays. The investigation showed that small structures, not normally well defined using conventional microscopy, can be resolved and identified with the atomic force microscope. Furthermore, the height information gathered by atomic force microscopy is useful for eliminating counting mistakes, which might be caused by chromatid or chromosome overlaps. The superior resolution of atomic force microscopy over conventional optical microscopy renders the scoring of as few as 20 cells per dose point as sufficient to draw accurate dose curves that correctly express the biological damage induced by different radiation sources.

Introduction

The absorption of ionizing radiation by cells results in the formation of chromosomal aberrations. A common technique to observe these abnormalities is fluorescence microscopy (FM),[1–5] which has a superior resolution to conventional optical microscopy. More detailed studies of chromosomal aberrations with higher resolution can be carried out with scanning electron microscopy (SEM).[6,7] The disadvantage of both these methods is, however, that the samples have to be subject to complicated staining or coating procedures before they can be analysed, and in the case of the SEM, measurements can be performed only in vacuum.

The atomic force microscope (AFM) enables contactless *in situ* measurements under ambient conditions and even in liquid, without any previous treatment of the sample. Furthermore, the lateral resolution of the AFM is superior to the SEM, in the ångström range and this allows the study of very small structures, such as DNA strands.[8–12]

Murakami *et al.*[6] used this nanometre resolution to demonstrate that the frequency of open and linear forms of plasmid DNA is related to radiation dose. Several other publications show that the AFM is a powerful tool to image the chromosome surface.[13] With this superior resolution, even the aberrations of small chromosomes, as found in some invertebrate species for example, can be observed, which is not always possible with conventional FM techniques. Furthermore, the high resolution of the AFM allows the investigator to classify aberrations correctly, thus making it possible to investigate fewer cells, yet maintaining the accuracy of statistical estimates. By quantifying different aberration types in response to the absorption of radiation energy, the use of the AFM presents a novel approach to relating chromosomal damage to the radiation dose and linear energy transfer (LET).

In the study reported here, AFM was used to determine a variety of chromosomal aberrations in Chinese hamster ovary cells and to establish a relationship between the frequency of aberrations and the radiation dose. High-resolution dose curves of radiation damage caused by gamma-ray and neutron irradiation were compared to ascertain if AFM observations were suitable to identify biological damage characteristic of different radiation sources. The main advantage of the AFM, however, is that the number of cells investigated to obtain statistically significant numbers of aberrations is considerably smaller than for other techniques, like FM, for which usually up to 500 cells are scored for one data point, whereas with the AFM the corresponding number was only 20 cells.

Materials and methods

Cell culturing

Chinese hamster ovary cells (CHO-K1), with a modal chromosome frequency of 23 (ATCC Rockville), were used in all experiments. These cells were cultured as a monolayer in Alpha Minimum Essential Medium, supplemented with 10% fetal calf serum and penicillin/streptomycin (0.1 mg/ml), and incubated at 37°C with 5% CO_2 in air.

Cell synchronization

To overcome the problem of differences in radiosensitivity during the various phases of the cell cycle, a simple method was employed to partially synchronize the cells.[4] In total, 2×10^5 cells were seeded in a 25-cm^2 tissue culture flask and grown to confluence over 72 h. At confluence, cells reached a stationary phase and were therefore arrested in G1. Cells were then trypsinized and subcultured by seeding 10×10^5 cells in 75-cm^2 flasks for neutron irradiation and 3×10^5 cells in 25-cm^2 flasks for gamma irradiation. Cells were incubated again and allowed 1–2 h to attach, before irradiation.

Irradiation

For gamma irradiation, an Eldorado-76 Cobalt-60 Teletherapy unit was used. The unit was directed upwards and build-up material was a 6-mm-thick Perspex table on which the samples were placed in a 30×30 cm^2 field, with a thick backscatter block of Perspex fixed directly above. The dose rate at the position of the sample was 0.33 Gy/min.

For neutron exposures, the p(66)/Be neutron therapy facility at iThemba LABS was used. The beam was directed downwards and samples were placed in a 30×30 cm^2 field on a 9-cm-thick backscatter block of Perspex. Build-up material consisted of 20 mm polyethylene and the dose-rate at the samples was ~0.4 Gy/min.

Samples were irradiated with γ-ray and neutron dosages of 2–7 Gy and 1–3 Gy, respectively.

Chromosome preparation

After irradiation, the cell cultures were incubated for about 20 h to allow cells to reach mitosis. During this phase cells round up and become loosely attached to the growth surface. Cells were detached by gently shaking the culture flasks. The mitotic cell suspensions were then transferred to centrifuge tubes for chromosome preparation. Suspensions were centrifuged and cells resuspended in hypotonic solution (75 mM KCl) and left for 20 min at 37°C. The cells were then fixed in a methanol:acetic acid mixture (3:1), according to a standard chromosome preparation technique.[14] For each sample the cell suspension was dropped onto a 22×22 mm^2 ice-cold glass cover slip and dried with hot air. The positions of metaphase spreads were marked, using a phase contrast microscope at ×400 magnification.

Imaging

The AFM scans were obtained with a Topometrix Explorer, operated in the high-amplitude non-contact mode under ambient conditions. The silicon cantilever[15] had a resonance frequency of about 170 kHz and was operated with a drive amplitude of 0.8 V. Images were obtained with a scan size of $50 \times 50\,\mu$m and a scan speed of two lines per second. The acquired images were processed with the internal Topometrix imaging program.

Evaluation

Cells in metaphase were analysed for dicentrics and rings. Polycentric chromosomes

[a]UNESCO Associated Centre for Macromolecules and Materials, Department of Chemistry and Polymer Science, University of Stellenbosch, Private Bag X1, Matieland 7602, South Africa.

[b]iThemba Laboratories for Accelerator Based Sciences, Radiation Biophysics Group, P.O. Box 722, Somerset West 7129, South Africa.

*Author for correspondence. E-mail: mmein@sun.ac.za

and sister unions were counted respectively as dicentrics and rings. About 20 metaphase spreads were scored for each sample and the average number of aberrations per cell plotted as a function of the dose. Polycentric chromosomes and ring structures were plotted separately.

Results and discussion

The quality of typical AFM images is demonstrated in Fig. 1, which displays a chromosome during metaphase (a) and several aberrations, such as a dicentric chromosome (b), a tricentric chromosome (c), an acentric ring (d) and a sister union (e).

The achievable resolution of the AFM is considerably higher than the images in Fig. 1 suggest, but since this study was mainly concerned with the number of aberrations from the common metaphase form among all chromosomes in one cell, the scans were taken with low magnification.

Two advantages of the AFM over FM are apparent: 1) small structures, which might be mistaken for something else in the FM image, can be resolved and identified; 2) overlaps of chromosomes or chromatids could be mistaken for aberrations in FM images but can be visualized with the AFM.

Figure 2 shows the same chromosomes scanned with the AFM (a) and observed through the FM (b). This example shows clearly that some chromosome structures are not resolved in the FM image. Structures like small rings might be mistaken for chromosome fragments if observed using techniques with a low resolution. The ring in the image, marked by an arrow, has a diameter of only 2 μm and in the AFM image is clearly displayed as a ring, whereas in the fluorescence microscope image it appears as an acentric fragment of a chromosome.

Figure 3 shows examples of overlapping chromosomes or chromatids that might easily be mistaken for dicentrics (a) or rings (b). In Fig. 3a one chromatid overlaps the other, which appears as a second centromere (marked with an arrow). Since the AFM image yields height information, it can clearly distinguish between centromeres and overlaps. Figure 3b shows two chromosomes overlapping. The larger chromosome is bent and touches the smaller chromosome, which is lying on top of it. Without height information and the resolution from the AFM, this structure might appear as a sister union.

These artifacts could lead to false statistics if aberrations per cell are scored with the FM. This statistical error can only be overcome by a high enough number of scores, which is commonly between 500 and 1000.

In the AFM results presented here, the average number of cells scored per sample was 20, since this method is likely to detect even small aberrations reliably. For AFM analysis, each of the 20 marked

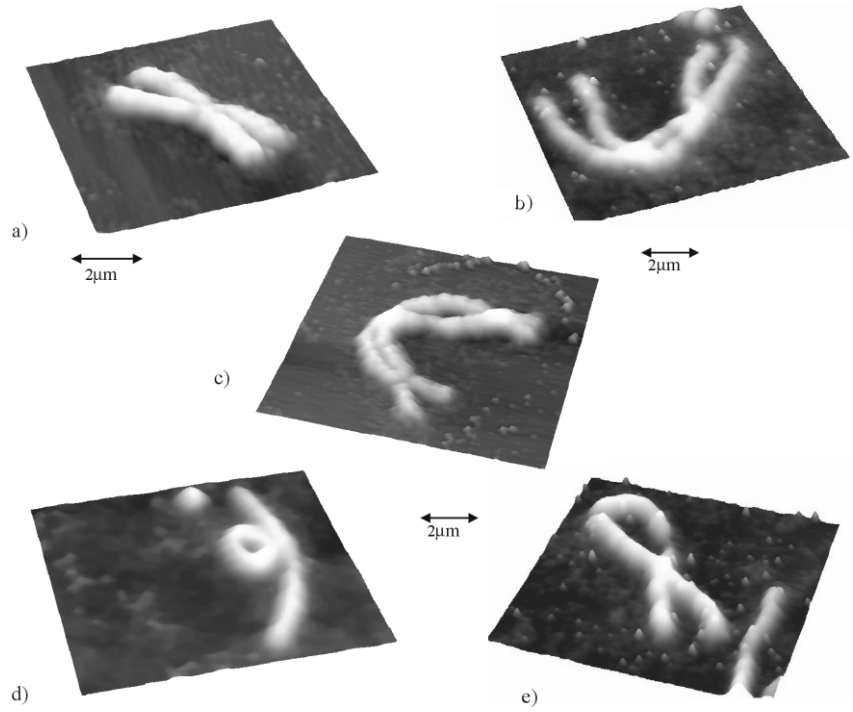

Fig. 1. a, A metaphase chromosome and different aberrations; **b**, a dicentric, **c**, a tricentric, **d**, an acentric ring and **e**, a sister union.

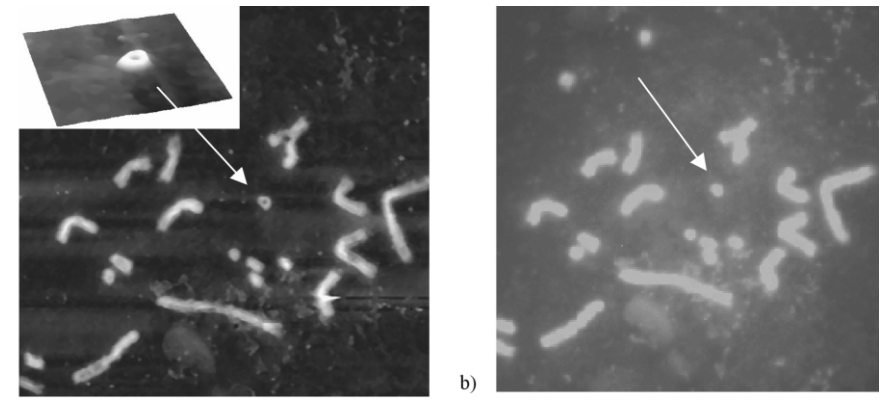

Fig. 2. The same chromosomes imaged by (**a**) AFM and (**b**) FM. The inset in the AFM image shows a small ring, which cannot be resolved with the FM. The image size is 50 µm^2.

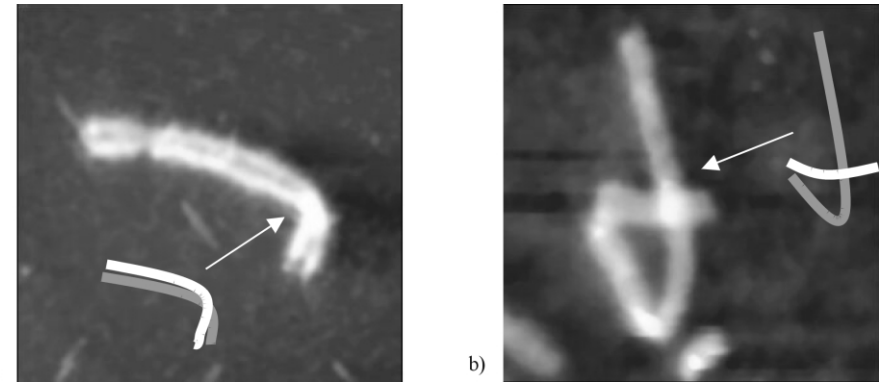

Fig. 3. Overlapping chromosomes or chromatids that might be mistaken for a (**a**) dicentric or (**b**) sister union. The image size is 20 µm^2.

metaphase spreads for each dose point was scanned and the number of aberrations per cell counted. The number of dicentrics (polycentrics) and rings per cell were then plotted as a function of the radiation dose, after the number of aberrations per cell counted in an unirradiated control sample was subtracted.

With high LET radiation, like the neutrons used in this study, a linear relationship between dose and the number of aberrations is expected, since the breaks in the two chromatids are the result of one ionizing particle. By contrast, the relationship is linear-quadratic for γ-irradiation.[16,17] For low doses the linear term prevails and the damage in the chromosome is believed to originate from one electron. At a higher dose the two breaks are more likely to be caused by two different electrons, which leads to the quadratic relationship. Monte Carlo simulations by Chen *et al.*[18,19] predict the number of chromosome breaks and exchange-type chromosomal aberrations for different radiation types. Studies by Ottolenghi *et al.*[20] describe the influence of the nuclear and chromosomal structure on chromosome aberrations. Figure 4 shows the results of the AFM measurements.

The experimental data on the aberrations per cell obtained from this study were fitted with a linear aberration-dose relationship for neutron irradiation and with a linear-quadratic relationship for γ-irradiation. The rings per cell and the dicentrics per cell were plotted as a function of the dose (Fig. 4).

For both radiation types the number of dicentrics per cell was generally higher than the number of rings per cell, but they followed the same trend. For γ-radiation the relationship was, as expected, linear-quadratic and could be fitted to the curve $y = \alpha.D + \beta.D^2$, where D is dose. For neutron irradiation, the relationship between the number of aberrations and the dose was linear, and could be fitted to a curve of the form $y = \alpha.D$. The fit parameters obtained from this study are listed in Table 1.

The number of aberrations scored in the cells irradiated with neutrons and γ-rays agrees well with other studies, such as that by Roberts *et al.*[4] They irradiated CHO cells with neutrons and γ-rays and scored the number of aberrations per cell with FM and fitted the data to the same curves as mentioned above. All fit parameters of their study were found to be of the same order as those in Table 1. This suggests that aberration numbers per cell obtained by AFM are as reliable as the numbers scored by FM, whereas the advantage of the AFM lies in the low number of cells that need to be investigated to obtain statistically significant values. The implicit time saving, since fewer cells per sample need to be investigated, is a further advantage of the AFM method.

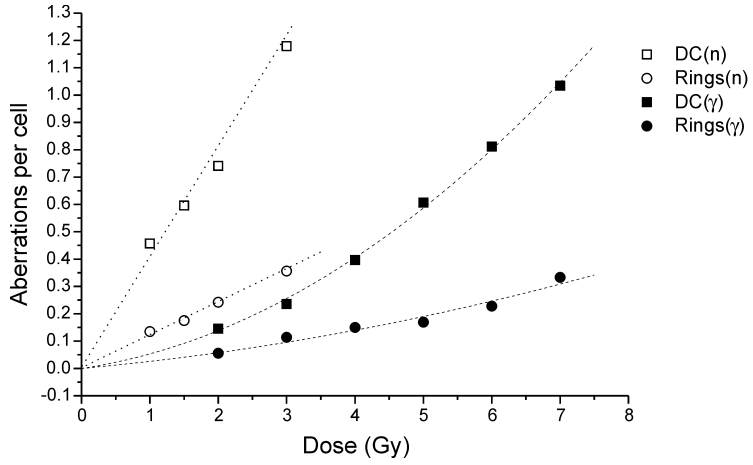

Fig. 4. Aberrations per cell as a function of dose for neutron- and γ-irradiation. The dotted lines are the fitted functions.

As the ionization density of neutrons is much higher than that of γ-rays, a higher frequency of multiple damage to single chromosome (ring formations) can be expected for the same dose compared to two chromosomes (dicentrics). The 2- and 3-Gy dose samples are comparable for both irradiation types used in this investigation. For this, a ratio of dicentrics to rings of 3.7 and 2.5 was noted for γ-rays, while that for neutrons was only 2.4 and 1.8, for 2 and 3 Gy, respectively (Table 2). AFM observations made in this study are therefore consistent with the microdosimetric nature of the radiation involved.

Table 1. Fit parameters for neutron (α) and γ-irradiation (α, β) for the number of rings and dicentrics (DC) per cell.

Aberration type	α	β
DC (γ-rays)	0.036 ± 0.008	0.0165 ±0.001
Rings (γ-rays)	0.173 ±0.007	0.007 ±0.001
DC (neutrons)	0.417 ±0.033	–
Rings (neutrons)	0.221 ±0.011	–

The biological effectiveness of p(66)/Be neutrons relative to ^{60}Co γ-rays (RBE) for CHO-K1 cells was estimated by comparing the fraction of cells noted without any type of aberration as a function of dose. From this a RBE value of 2.3 was estimated, which agrees with that of other cell types exposed to the same neutron energy.[21,22]

Table 2. Frequency and distribution of dicentrics and rings in CHO-K1 cells as scored with the AFM, after irradiation with neutrons and γ-rays.

Radiation modality	Aberration type	Dose (Gy)	Aberrations/ cell	Cells scored	Distribution			
					0	1	2	3
Neutrons	Dicentrics	0	0.08	13	1	2	1	
		1	0.72	18	8	7	3	
		1.5	0.80	20	8	9	2	1
		2	0.90	21	9	7	3	2
		3	1.22	18	3	8	7	
	Rings	0	0.00	13	13			
		1	0.22	18	14	4		
		1.5	0.40	20	14	4	2	
		2	0.38	21	15	5		1
		3	0.67	18	8	8	2	
γ-rays	Dicentrics	0	0.08	13	12	1		
		2	0.22	18	14	4		
		3	0.31	16	12	3	1	
		4	0.45	20	11	9		
		5	0.68	19	10	6	2	1
		6	0.83	18	8	5	5	
		7	1.11	18	5	6	7	
	Rings	0	0.00	13	13			
		2	0.06	18	17	1		
		3	0.13	16	14	2		
		4	0.20	20	16	4		
		5	0.26	19	14	5		
		6	0.33	18	12	6		
		7	0.50	18	9	8	1	

Conclusion

The AFM proved to be very useful for quantifying different types of chromosome aberrations following exposure of cells to graded doses of radiation and to different ionization densities. Dicentric and ring frequencies observed in relatively few metaphase spreads gave dose–response curves that reflect both the quantity of radiation energy absorbed as well as the ionization density of the treatment modality. The high resolution of AFM images allows exact identification of aberrant structures and could prove to be particularly valuable for analysing small chromosomes, characteristic of some lower order species.

We thank J. Symons of iThemba LABS for the dose calibration of the p(66)/Be neutron irradiation set-up, and the National Research Foundation for funding.

1. Volkmer B. and Virsik-Peuckert R. (1990). Kinetics of chromosome lesion repair in synchronized quiescent and proliferating CHO cells. *Int. J. Radiat. Biol.* **58**, 1009–1023.
2. Deng W., Morrison D., Gale K. and Lucas J. (2000). A comparative study on potential cytogenic fingerprints for radiation LET in human lymphocytes. *Int. J. Radiat. Biol.* **76**, 1589–1598.
3. Sasaki M., Kobayashi K., Hieda K., Yamada T., Ejima Y., Maezawa H., Furusawa Y., Ito T. and Okada S. (1989). Induction of chromosome aberration in human lymphocytes by monochromatic X-rays of quantum energy between 4.8 and 16.6 keV. *Int. J. Radiat. Biol.* **56**, 975–988.
4. Roberts C. and Holt P. (1982). The production of chromosome aberration in Chinese hamster fibroblasts by gamma and neutron irradiation. *J. Int. Radiat. Biol.* **41**, 645–656.
5. Dikomey E. and Franzke J. (1992). Effect of heat on induction and repair of DNA strand breaks in X-irradiated CHO cells. *Int. J. Radiat. Biol.* **61**, 221–233.
6. Murakami M., Hirokawa H. and Hayata I. (2000). Analysis of radiation damage of DNA by atomic force microscopy in comparison with agarose gel electrophoresis studies. *J. Biochem. Biophys. Meth.* **44**, 31–40.
7. Herskind C. (1987). Single strand breaks can lead to complex configuration of plasmid DNA in vitro. *Int. J. Radiat. Biol.* **52**, 565–575.
8. Hansma H., Hoh J. (1994). Biomolecular imaging with the atomic force microscope. *Annu. Rev. Bioph. Biom.* **23**, 115–139.
9. Hansma H. (2001). Surface biology of DNA by atomic force microscopy. *Annu. Rev. Phys. Chem.* **52**, 71–92.
10. Chen C. and Hansma H. (2000). Basement membrane macromolecules: insights from atomic force microscopy. *J. Struct. Biol.* **131**, 44–55.
11. Pang D., Berman B., Chasovskikh S., Rodgers J. and Dritschilo A. (1998). Investigation of neutron induced damage in DNA by atomic force microscopy: experimental evidence of clustered DNA lesions. *Radiat. Res.* **150**, 612–618.
12. Hecker H., Betschart B., Burri M. and Schlimme W. (1995). Functional morphology of trypanosome chromatin. *Parasitol. Today* **11**, 79–83.
13. Tamayo J. and Miles M. (2000). Human chromosome structure studied by scanning force microscopy after an enzymatic digestion of the covering cell material. *Ultramicroscopy* **82**, 245–251.
14. Freshney R. (1983). In *Culture of Animal Cells: A manual of basic techniques,* pp. 165–167. Alan R. Liss, New York.
15. Nanosensors (2000). *Product specification.* Nanosensors, Neuchatel, Switzerland.
16. Natarajan A. (2002). Chromosome aberrations: past, present and future. *Mutat. Res.* **504**, 3–16.
17. Obe G., Pfeiffer P., Johannes C., Goedecke W., Jeppesen P., Natarajan A., Martinez-Lopez W., Folle G. and Drets M. (2002). Chromosomal aberrations: formation, identification and distribution. *Mutat. Res.* **504**, 17–36.
18. Chen A., Lucas J., Simpson P., Griffin C. *et al.* (1997). Computer simulation of data on chromosome aberrations produced by X-rays or α particles and detected by fluorescence in situ hybridization. *Radiat. Res.* **148**, 93–101.
19. Ottolenghi A., Ballarini F. and Merzagora M. (1999). Modelling radiation induced biological lesions: from initial energy depositions to chromosome aberrations. *Radiat. Environ. Biophys.* **34**, 1–13
20. Ottolenghi A., Ballarini F. and Biaggi M. (2001). Modelling chromosomal aberration induction by ionizing radiation: the influence of interphase chromosome architecture. *Adv. Space Res.* **27**, 369–382.
21. Slabbert J., Theron T., Serafin A., Jones D., Böhm L. and Schmitt G. (1996). Radiosensitivity variations in human tumor cell lines exposed *in vitro* to p(66)/Be neutrons or ^{60}Co-rays. *Strahlenther. Onkol.* **172**, 567–572.
22. Slabbert J., Theron T., Zoelzer F., Streffer C. and Boehm L. (2000). A comparison of the potential therapeutic gain of p(66)/Be neutrons and d(14)/Be neutrons. *Int. J. Oncol. Biol. Phys.* **47**, 1059–1065.